Energy Reports 8 (2022) 10833–10848

Contents lists available at ScienceDirect

Energy Reports

journal homepage: www.elsevier.com/locate/egyr

Research paper

A high-temperature heat pump for compressed heat energy storage applications: Design, modeling, and performance

Abdelrahman H. Hassan [a,b], José M. Corberán [a], Miguel Ramirez [c], Felipe Trebilcock-Kelly [c], Jorge Payá [a,*]

[a] Instituto Universitario de Investigación en Ingeniería Energética, Universitat Politècnica de València, 46022, Valencia, Spain
[b] Mechanical Power Engineering Department, Faculty of Engineering, Zagazig University, Zagazig 44519, Egypt
[c] Tecnalia Research & Innovation, Energy and Environment Division, Area Anardi 5, Azpeitia, Guipuzkoa 20730, Spain

ARTICLE INFO

Article history:
Received 16 May 2022
Received in revised form 19 July 2022
Accepted 14 August 2022
Available online 2 September 2022

Keywords:
Pumped thermal energy storage
High-temperature heat pump
Modeling
Subcooling
Superheat
Refrigerants

ABSTRACT

The current paper presents the design and performance of a high-temperature heat pump (HTHP) integrated in an innovative, sensible, and latent heat storage system. The HTHP has been designed to work between a heat source from 40 to 100 °C and a heat sink above 130 °C. An initial refrigerant analysis has revealed that R-1233zd(E) is the best candidate to meet the required performance and environmental considerations. The first part of this paper deals with the sizing and selection of the main components while discussing the challenges and working limits. A numerical model is also presented and validated. The second part of the paper is dedicated to develop parametric studies and performance maps under different operating conditions. The results show that the current HTHP, at a source temperature of 80 °C, consumes from 3.23 to 9.88 kW by varying the compressor's speed from 500 to 1500 rpm. Heat production is achieved in the form of latent heat (7.40 to 21.59 kW) and sensible heat (from 6.35 to 17.94 kW). The heating coefficient of performance (COP_{HTHP}) is around 4.

© 2022 The Authors. Published by Elsevier Ltd. This is an open access article under the CC BY-NC-ND license (http://creativecommons.org/licenses/by-nc-nd/4.0/).

1. Introduction

Reducing the CO_2 emissions is becoming a major engineering challenge given the increasing world population, and the growing demand of energy. Generation of electricity with renewable energies, or with fuel cells can contribute to reduce the global warming (Barnoon, 2021; Barnoon et al., 2022; Mei et al., 2022). However, due to the mismatching between generation and demand, cost-effective energy storage solutions are essential, as discussed by Lu et al. (2021) in a recent special issue on energy storage for the time period 2019–2020. A significant effort is being applied in the development and testing of batteries. For instance, Dascalu et al. (2022) recently carried out an experimental analysis of a three year dataset of 2019 to 2021 with a hybrid battery of li-ion and lead–acid. Energy storage not only requires a specific attention on individual devices, but also on full systems, as recently reviewed by al Shaqsi et al. (2020). Feng et al. (2022) explored a distributed renewable energy and hybrid energy storage system including a battery, super capacitor and compressed air energy storage (CAES). Meng et al. (2021) studied the most relevant factors for the development of energy storage in renewable energy projects.

Thermal energy storage (TES) is also one of the bottlenecks for a further penetration of renewable energies. For instance, the use of molten salts in concentrating solar power plants can help produce electricity 24h/day owing to the sensible heat energy storage. There are many examples of applications of sensible heat storage, for instance Doretti et al. (2020) who analyzed numerically the effect of the modules' arrangement using concreted thermal storage. Huang et al. (2020) investigated the thermal management of lithium-ion batteries depending on different phase-change material (PCM) parameters. Gluyas et al. (2020) showed that there is a great potential in the UK for the development of large-scale underground thermal energy storage.

The present work has been developed within the frame of the EU project "Compressed Heat Energy STorage for Energy from Renewable sources" (CHESTER) (grant agreement No. 764042).[1] The CHESTER project aims to develop an innovative compressed heat energy storage (CHEST) system for efficient storage and dispatching of energy from renewable energy sources (RES). One of the key components of this system is a High Temperature Heat Pump (HTHP) capable of pumping heat at high sink temperatures (> 130 °C).

HTHPs are starting to be considered a potential key technology for the industry (Hassan et al., 2020), especially for saturated/superheated steam generation (Li et al., 2021). In fact,

* Corresponding author.
E-mail address: jorge.paya@iie.upv.es (J. Payá).

[1] https://www.chester-project.eu/.

https://doi.org/10.1016/j.egyr.2022.08.201
2352-4847/© 2022 The Authors. Published by Elsevier Ltd. This is an open access article under the CC BY-NC-ND license (http://creativecommons.org/licenses/by-nc-nd/4.0/).

Nomenclature

CC	cooling capacity [kW]
COP_{HTHP}	heating coefficient of performance [-]
DSH	desuperheating [K]
FC	friction coefficient [-]
GWP	global warming potential [-]
h	specific enthalpy [kJ/kg]
HTC	heat transfer coefficient [W/m^2 K]
LHC	latent heat capacity [kW]
m	mass flow rate [kg/s]
M	molar mass [kg/kmol]
NBP	normal boiling point [°C]
n_{comp}	compressor's speed [rpm]
η_{is}	isentropic efficiency [-]
η_o	overall efficiency [-]
NoP	number of heat exchanger's plates [-]
ODP	ozone depletion potential [-]
η_v	volumetric efficiency [-]
p	pressure [kPa]
P_{el}	electrical power [kW]
Φ_{loss}	compressor's heat losses [%]
Pr	pressure ratio [-]
Q	heat transfer rate [kW]
R_{uni}	universal gas constant [kJ/kmol.K]
SC	subcooling [K]
SH	superheat [K]
SHC	sensible heating capacity [kW]
T	temperature [°C]
THC	total heating capacity [kW]
v	specific volume [m^3/kg]
V_{ch}	channel volume of the heat exchanger [L]
V_d	compressor's total displacement [m^3/rev]
Δp	pressure difference [kPa]
ΔT	temperature difference [K]
ρ	density [kg/m^3]

Subscripts

avg	average
comp	compressor
cond	condensation/condenser
crit	critical
dis	discharge
evap	evaporation/evaporator
HTHP	high-temperature heat pump
in	inlet
is	isentropic
loss	losses
max	maximum
melt	melting
min	minimum
ORC	organic Rankine cycle
out	outlet
PCM	phase change material
ref	refrigerant
snk	sink
src	source
subc	subcooler
suc	suction
w	water

industrial processes are currently responsible for around 21% of the total CO_2 emissions in Europe (de-Boer et al., 2020). The majority (66%) of the industrial energy use is for process heating purposes, and the energy source is mainly from non-renewable energy sources (77%). In particular, the temperature range from 100 to 200 °C requires around 26% of the total process heat demand and is mainly produced with fossil fuel burners. Given the current Green Deal objectives and to make Europe carbon-neutral and resource efficient by 2050.

Previous studies have shown that industrial heat pumps have the potential to cover around 28.37 TWh/a in European Union (EU) industries (Kosmadakis, 2019) and to reduce CO_2 emissions by 67% (de-Boer et al., 2020). Compared to gas boilers, heat pumps can reach a better efficiency and at the same time recover waste heat, which according to Papapetrou et al. (2018), is around 1.25 TWh/a in the EU industries for temperatures below 100 °C. Kosmadakis et al. (2020) showed that payback periods below two years could be potentially reached in some countries such as Finland or Sweden.

Nowadays, only a limited number of manufacturers can provide systems to produce process heat above 100 °C. The current temperature limit of commercial heat pumps is of around 120–130 °C. Some examples are Kobelco's SGH120 vapor-compression heat pump, which produces saturated steam at 120 °C (Kaida et al., 2015), and Mayekawa's Eco Sirocco CO_2 heat pump air heater, which consists of a CO_2 transcritical cycle to heat the air up to 120 °C (MAYEKAWA, 2022). OCHSNER (2022) offers heat pumps such as IWWDS ER3b, which can achieve 130 °C in the condenser outlet. The German manufacturer SPH states they can reach heat sink temperatures of up to 165 °C with heat source temperatures of up to 120 °C (SPH, 2022).

The challenges to be faced by HTHPs are mainly related to the high discharge temperatures. Lubrication and proper oil cooling are essential to ensure a long lifetime. The electrical motors could also be larger due to the need for high torques.

The biggest challenge of HTHPs is the compressor, as discussed in more detail within the present work. Most of the HTHP prototypes that have been tested up-to-date employ piston/reciprocating compressors (Arpagaus et al., 2019; Bamigbetan et al., 2019; Fleckel, 2015); and a few use screw compressors (EDF, 2015; Mateu-Royo et al., 2019). To solve the problems of lubrication and to reach better efficiencies, particularly for MW scale applications, turbocompressors seem to be the most interesting option.

The current paper focuses on designing the mentioned HTHP, mapping its performance under different working conditions, and discussing the main challenges and operational limits.

In comparison to the current state-of-the-art, the present work incorporates the following novelties:

- Presenting a detailed physical-based HTHP model, with real size and specification of each component, instead of using simple thermodynamic steady-state models, as in the case of many published works regarding similar HTHPs.
- Introducing the subcooler as a key component to store the sensible heat available from the hot liquid refrigerant after the condenser.
- Optimizing the superheat inside the evaporator.
- Quantifying the impact of the compressor's heat losses.
- Evaluating the partial load performance of the HTHP.

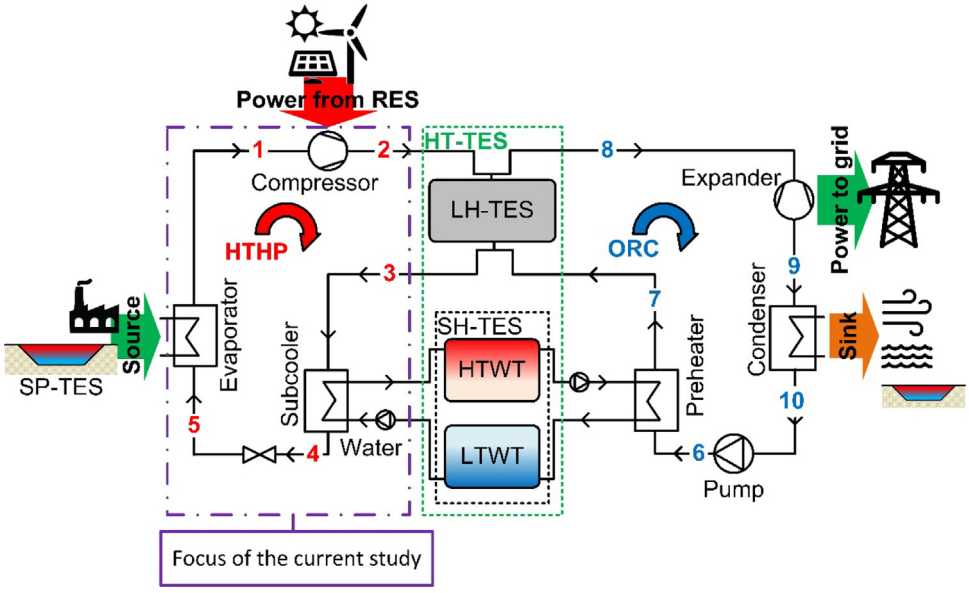

Fig. 1. CHEST system concept.

2. CHEST system concept and design methodology

The CHEST system consists of three main components, as seen in Fig. 1. The HTHP pumps heat from low- or medium-temperature sources, such as industrial waste heat, seasonal pit thermal energy storage (SP-TES), etc., to a high-temperature thermal energy storage (HT-TES). The electrical power required to drive the HTHP should come from RES when available. The organic Rankine cycle (ORC) acts as a heat engine to transform the stored thermal energy into electricity when needed.

The HT-TES in Fig. 1 comprises two sub-storage systems. The first sub-storage is the latent heat thermal energy storage (LH-TES) which contains a bundle of finned-tubes immersed in a tank filled with PCM to allow storing the thermal energy in the form of latent heat. The LH-TES is either the HTHP's condenser during the charging cycle, or the ORC's evaporator during the discharging cycle.

The second sub-storage is the sensible heat thermal energy storage (SH-TES) which comprises two pressurized water tanks to allow the sensible heat transfer between the water and the refrigerant during charging and discharging cycles.

The CHEST system should work between the source temperature range of 40–100 °C and the sink temperature range of 10–60 °C (Hassan et al., 2020; Pascual, 2019). This wide range of operating conditions makes the CHEST system very flexible and eases the integration with other thermal systems, such as with district heating networks.

As a requirement of the CHESTER project, the HTHP's electrical consumption for the lab-scale system should be within 10–15 kW. The PCM melting temperature defines the maximum temperature limit for the HT-TES system and, subsequently, the HTHP's condensation temperature. A eutectic mixture of potassium nitrate and lithium nitrate (KNO_3-$LiNO_3$), with a melting temperature of $T_{melt,PCM} = 133$ °C, was selected for the latent heat storage system.

The selection of the refrigerant (Section 3.1) has been performed owing to a previous study by Corberán et al. (2019), using a steady-state thermodynamic model in Engineering Equation Solver (EES) (Klein, 2019). The compressor has been selected (Section 3.2), giving priority to robust solutions which can withstand the necessary power and discharge temperatures with efficient lubrication. The detailed heat exchangers were selected (Section 3.3) using both the EES-CHEST model (Hassan et al., 2020) and the SWEP's SSP-G8 selection tool (SWEP International AB, 2019). Finally, the IMST-ART tool (IMST-ART, 2010) was employed to model the HTHP (Section 4) and to characterize the system performance under different operating conditions (Section 5).

3. HTHP'S design and components

Based on the working limits of the lab-scale CHEST system discussed in Section 2, the nominal working point for the HTHP is defined as follows:

- Inlet source temperature for the HTHP ($T_{src,in,HTHP}$) = 80 °C.
- Source temperature lift in the HTHP's evaporator ($\Delta T_{src,HTHP}$) = 5 K.
- Condensation temperature ($T_{cond,HTHP}$) ≥ 138 °C (to ensure a proper condensation inside the LH-TES).
- Inlet water temperature to the HTHP's subcooler ($T_{w,in,subc}$) = 60 °C.

The main focus of the present work is the detailed design and expected performance of the HTHP itself, as a single equipment works with vapor-compression cycle. The individual, stand-alone development and characterization of the HTHP has been performed in Spain, in the laboratories of TECNALIA (who is the partner responsible for building and testing the HTHP). The LH-TES and the SH-TES are part of the full CHEST system for the conversion of electricity-to-heat-to-electricity. However, an individual characterization of the HTHP requires to decouple it from the rest of the CHEST system. For this reason, in TECNALIA, the LH-TES was replaced with a brazed plate heat exchanger (BPHX) condenser, as seen in Fig. 2. Pressurized water, at high flow rates, is utilized a secondary fluid to mimic the PCM behavior. After shipping the HTHP to the DLR's facilities in Germany (the partner responsible for integrating and testing the whole CHEST system), the BPHX condenser will be bypassed to allow the direct condensation of refrigerant inside the LH-TES system, as indicated in Section 2.

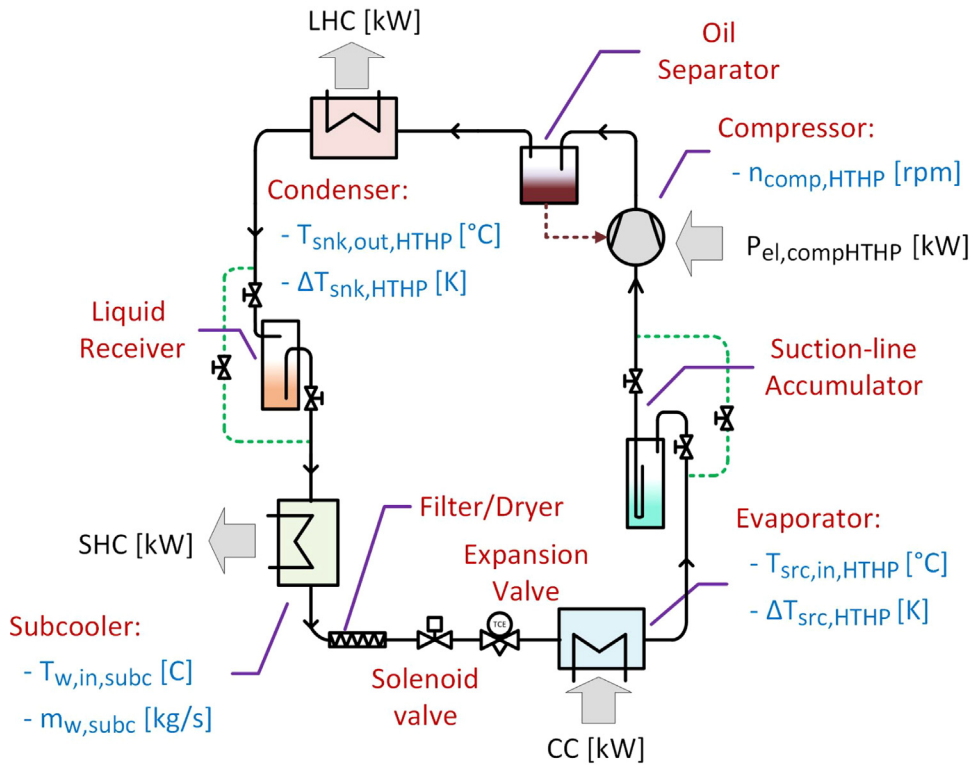

Fig. 2. Main components of the stand-alone HTHP, the flow of heat and work (in black), and independent variables (in blue). (For interpretation of the references to color in this figure legend, the reader is referred to the web version of this article.)

3.1. Comparison of potential refrigerants

One of the initial steps to design a HTHP is the selection of a proper working fluid that acts well under higher temperature lifts between evaporation and condensation temperatures.

As seen in Figs. 1 and 2, the CHEST system uses a subcooler after the condenser to obtain the maximum benefit from the hot liquid refrigerant after condensation. This helps to better match the temperature profiles between the refrigerant and the secondary fluid-side and to minimize the heat transfer irreversibilities. This particular configuration prevents the use of the internal, liquid-to-suction, heat exchanger (IHX) since the outlet of the subcooler in many scenarios could be at less than the suction temperature in the inlet of the compressor.

Thus, the only way to achieve the required superheat (SH), to prevent wet compression and to protect the compressor, is inside the evaporator itself. This is a crucial aspect that should be taken into account. The refrigerants that need high SH values result in very low evaporation temperatures and, subsequently, high pressure ratio values which could significantly degrade the system performance. This makes them unsuitable for the proposed HTHP and CHEST system.

Based on the previous discussion, some of the renowned refrigerants widely used for subcritical HTHP applications were initially analyzed (see Table 1). The physical properties of these refrigerants are given based on Lemmon et al. (2018). R-245fa is, nowadays, the most widely used refrigerant for HTHP applications and was hereby selected as the reference refrigerant in the current study. However, R-245fa yields the highest Global Warming Potential (GWP) among the chosen refrigerants of Table 1.

To compare the previous refrigerants, the experimental HTHP in Fig. 2 was simulated in EES for the nominal point. The following assumptions were employed:

- Steady-state conditions.
- No pressure drop inside heat exchanger or refrigerant lines.
- Constant pinch point (PP) of 5 K inside the heat exchangers.
- Constant compressor efficiency (η_{comp}) and compressor heat losses ($\varphi_{loss,comp}$) of 0.65 and 25%, respectively. These are typical values for piston compressors employed in HTHPs.
- The SH is varied to maintain a constant desuperheating of 5 K at the condenser's inlet, which prevents the wet compression phenomenon.
- Constant sink temperature = 133 °C (melting point of the given PCM).
- The outlet of the condenser is always saturated liquid.
- Constant evaporator capacity of 40 kW, based on a cooling COP of 4 and an inlet electrical power of 10 kW (the desired input for the lab-scale CHEST system).

Fig. 3 (up) shows the p-h diagram for the HTHP for the selected refrigerants, and (down) the comparison of the main performance parameters relative to the reference refrigerant (R-245fa). R-1336mzz(Z) has the highest SH value, ≈2.5 times higher than R-245fa, which, in turn, results in the lowest evaporation temperature, and in the highest pressure ratio (Pr). The relative volumetric heating capacity (VHC) is also very low (≈0.3). This means that to pump, for instance, 10 kJ of heat with the current HTHP using R-1336mzz(Z) as refrigerant, the compressor should be approximately three times bigger than with R-245fa in terms of displacement volume [m^3]. Even if R-1336mzz(Z) is the main candidate for many HTHP applications (Fleckl et al., 2015; Nilsson et al., 2017), it is not suitable in the current CHEST application, mainly due to the lack of IHXs.

Both R-1234ze(Z) and Butene require the lowest SH values in the current study, approximately 20% of the SH used for R-245fa. They also yield COP values ≈1.2 times higher than the COP of R-245fa. However, they have been excluded due to their flammability and to the low T_{crit}. In order to have the possibility of working with other PCMs with higher melting temperatures up to 150 °C, the critical temperature is also fundamental.

Table 1
List of potential refrigerants suitable for HTHP subcritical applications.

Refrigerant	Type	T_{crit} [°C]	p_{crit} [kPa]	NBP[b] [°C]	ODP[c] [-]	GWP [-]	SG[d]
R-245fa[a]	HFC[e]	**153.9**	**36500**	**15.1**	**0**	**1030**	B1
R-1336mzz(Z)	HFOs[f]	171.4	29000	33.4	0	2	A1
R-1233zd(E)	HCFOs[g]	166.5	36200	18.3	0	1	A1
R-1224yd(Z)	HCFOs	155.5	33400	14.6	0.00023	0.88	A1
R-600	HC[h]	152.0	38000	−0.5	0	4	A3
R-1234ze(Z)	HFOs	150.1	35300	9.7	0	<1	A2L
Butene	HC	146.1	40100	−6.3	0	<10	n.a.

[a]Reference refrigerant (REF).
[b]Normal boiling point at 101.3 kPa.
[c]Ozone depletion potential.
[d]Safety group (ASHRAE, 2016).
[e]Hydrofluorocarbons.
[f]Hydrofluoroolefins.
[g]Hydrochlorofluoroolefins.
[h]Hydrocarbons.

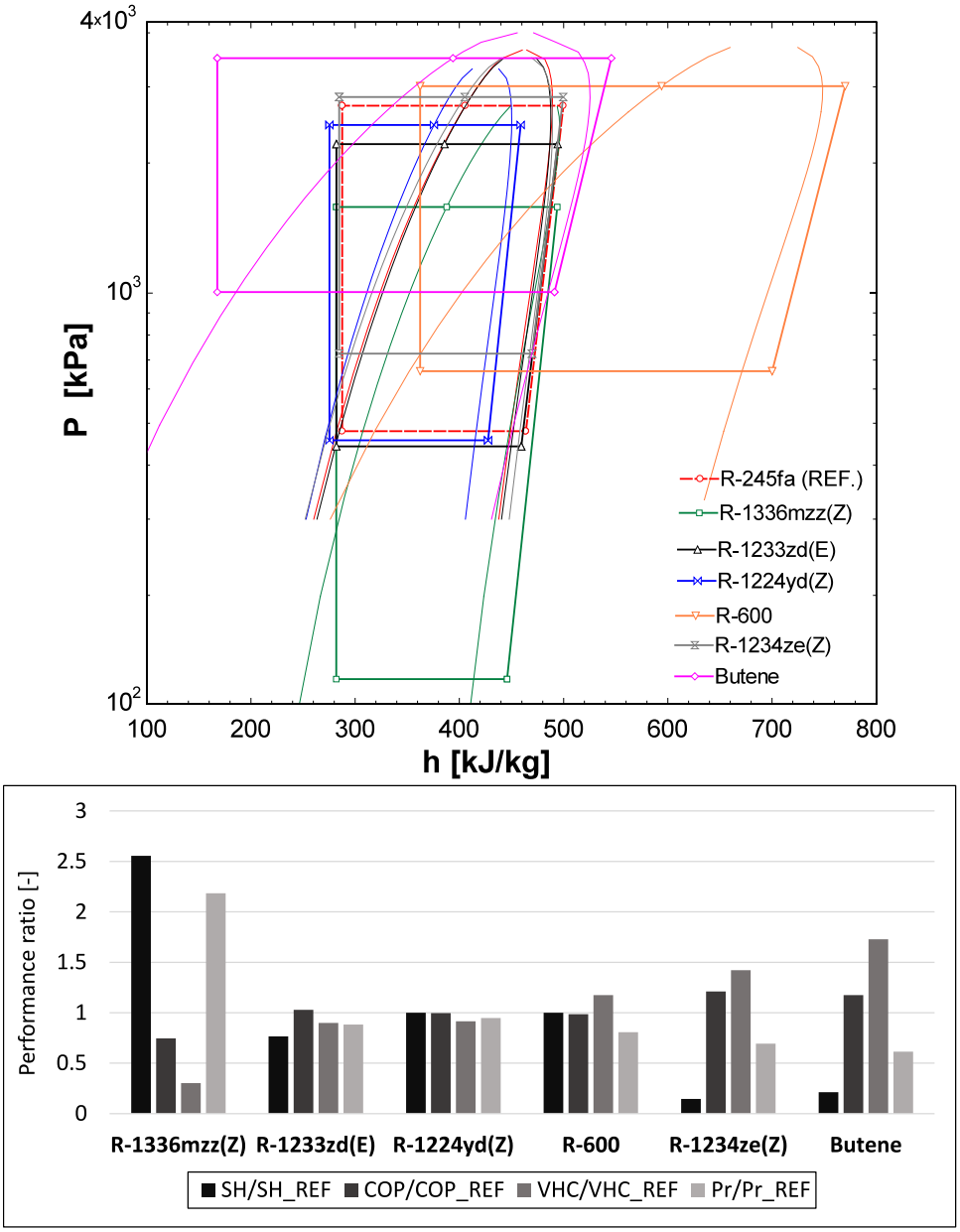

Fig. 3. (Up) p-h diagram for the selected refrigerants, and (down) comparison of performance parameters comparison relative to R-245fa (REF).

Among the assessed refrigerants, R-1233zd(E), R-1224yd(Z), and R-600 are the closest in performance to R-245fa. This means that they are potential candidates in HTHP applications as drop-in replacements for R-24fa. However, R-600 was excluded due to its flammability based on the ASHRAE designation for safety (ASHRAE, 2016). Finally, comparing R-1233zd(E) and R-1224yd(Z), Fig. 3 (down) shows that the results shift slightly in favor of R-1233zd(E) over R-1224yd(Z). In fact, R-1233zd(E) has 3 K less SH; 4.5% more COP; and 11 K more in T_{crit}, compared to R-1224yd(Z). Based on this detailed refrigerant analysis, R-1233zd(E) was finally selected as the primary working fluid for the experimental HTHP prototype.

3.2. Compressor selection and performance

The previous analysis in Section 3.1 indicates that the compressor should withstand a discharge temperature of 140 °C, at least. Working for many hours under these harsh conditions could degrade the lubricating oil and, finally, lead to compressor failure. Thus, as a literature survey of compressors has been carried out, with a special emphasis on similar HTHPs applications.

A 32 kWth HTHP using R-1336mzz(Z) was analyzed by Nilsson et al. (2017) using a specially designed reciprocating compressor from Viking Heat Engines (VHE). The HTHP was tested under a temperature lift from 20 to 60 K. The results showed that the compressor operated stably at all the measured temperature lifts, up to an outlet sink temperature of 150 °C. Bamigbetan et al. (2019) studied experimentally the performance of a prototype R-600 compressor for a HTHP. The tested compressor was a semi-hermetic, 4-cylinder piston compressor of Dorin S.p.A, delivering a total flow rate of 48.82 m^3/h. The condensation temperature was fixed between 114–118 °C, while the evaporation temperature was varied between 46–57 °C.

Mateu-Royo et al. (2019) evaluated a novel scroll open-type compressor modified by Expander Tech S.L for high-temperature applications using R-245fa as working fluid. This compressor is connected to a variable-speed motor of 7.5 kW nominal power and has a total displacement of 121.1 cm^3/rev. The results showed that for a sink temperature of 140 °C, the discharge temperature reached 160 °C.

Based on the previous survey, there is a lack of detailed experimental results of the compressor performance under high-temperature applications >130 °C, especially on the operational stability and endurance, for both compressor and lubricating oil, under long operating periods. For the current HTHP, the selected compressor was the HBC-511 model from VHE. The main specifications are given in Table 2. The main reason for choosing this specific compressor is that it is a robust, heavy-duty piston-type compressor designed especially for HTHP applications with elevated source and sink temperatures. Moreover, the required power range of 10–16 kW can be reached. The HBC-511 compressor can withstand maximum internal and discharge temperatures of 215 and 160 °C, respectively (Viking Heat Engines, 2018). Fig. 4 shows two photographs of the HBC-511 compressor in TECNALIA. The main specifications and dimensions are summarized in Table 2.

The manufacturer supplied the experimental performance data of the HBC-511 compressor using R-1336mzz(Z) as a refrigerant. The compressor was tested at a constant speed of 1500 rpm, Pr values from 2 to 6, inlet source temperatures from 73 to 111 °C, and outlet sink temperatures from 131 to 151 °C.

Based on this data, the regression tool of the Microsoft Excel program was used to obtain experimental performance correlations for the compressor. This tool is based on multiple linear regression using the sum of squares for the analysis of variance. The two main performance parameters are the refrigerant mass flow rate ($m_{ref,HTHP}$) [kg/s], Eq. (1), and the compressor inlet electrical power ($P_{el,comp,HTHP}$) [kW], Eq. (2). The accuracy of mentioned correlations is justified based on an adjusted $R^2 \geq 0.95$, and by the probability value of the independent variables ($\leq$0.05).

Table 2
Main specifications of VHE's HBC-511 compressor.

Feature	Single piston
Displacement [cm^3/rev]	511
Speed ($n_{comp,HTHP}$) [rpm]	500–1500
Working fluids [-]	HFCs and HFOs
Max. operating pressure (low-side) [kPa]	1000
Max. Operating pressure (high-side) [kPa]	3000
Max. Discharge temperature [°C]	160
Max. Internal temperature [°C]	215
Oil total volume [l]	7.5
Oil circulation rate [%]	0.5
Dimensions (L × W × H) [mm]	632 × 431 × 737
Weight [kg]	175
Rated electric power [kW]	15.5
Electrical motor efficiency [%]	92

$$m_{ref,HTHP} = (K_0 + K_1 \cdot p_{suc} + K_2 \cdot p_{dis}) \frac{n_{comp,HTHP}}{60} \cdot V_d \cdot \frac{M_{ref}}{R_{uni} \cdot (T_{suc} + 273.15)}, \quad (1)$$

with the fitted coefficients $k_0 = -1.060E{+}01$, $K_1 = 1.068E{+}00$, and $K_2 = -8.554E{-}02$

$$P_{el,comp,HTHP} = (C_0 + C_1 \cdot p_{suc} + C_2 \cdot p_{dis}) \frac{n_{comp,HTHP}}{60} \cdot V_d, \quad (2)$$

with the fitted coefficients $C_0 = 1.346E{+}02$, $C_1 = 8.143E{-}01$, $C_2 = 7.080E{-}02$.

p_{suc} and p_{dis} are, respectively, the suction and discharge pressures [kPa]. $n_{comp,HTHP}$ is the compressor speed [rpm]. V_d is the total displacement of the compressor [m^3/rev]. The universal gas constant (R_{uni}) [kJ/kmol K], suction temperature (T_{suc}) [°C], and refrigerant molar mass (M_{ref}) [kg/kmol] have been introduced as parameters since the selected refrigerant is R-1233zd(E) instead of the R-1336mzz(Z). Fig. 5 shows that Eqs. (1) and (2) predict well the experimental values of $P_{el,comp,HTHP}$ and $m_{ref,HTHP}$ for R-1336mzz(Z), within error bands of ±10%, with average absolute deviation values of ±1.6% and ±1.2%, respectively. These correlations will be later used to characterize the compressor in the HTHP simulations.

3.3. Heat exchangers sizing

To identify the required capacities of the heat exchangers, the whole system (Fig. 1) was modeled thermodynamically using the EES program. The detailed model (EES-CHEST), along with its validation, was recently presented by Hassan et al. (2020). The main assumptions of the EES-CHEST model are:

- The working fluid used for the HTHP, and ORC, is R-1233zd(E).
- The system always runs under steady-state conditions.
- No pressure drops are accounted inside the heat exchangers or connection pipes.
- The solidification and melting of the PCM are homogeneous, at $T_{melt,PCM} = 133$ °C.
- The ratios of sensible to latent heat during the charging and discharging processes are equal. In other words, there is no excess heat. All the heat produced by the HTHP is stored and later recovered to drive the ORC.
- The inlet to the HTHP's subcooler and the ORC's condenser outlet are always in a saturated state.

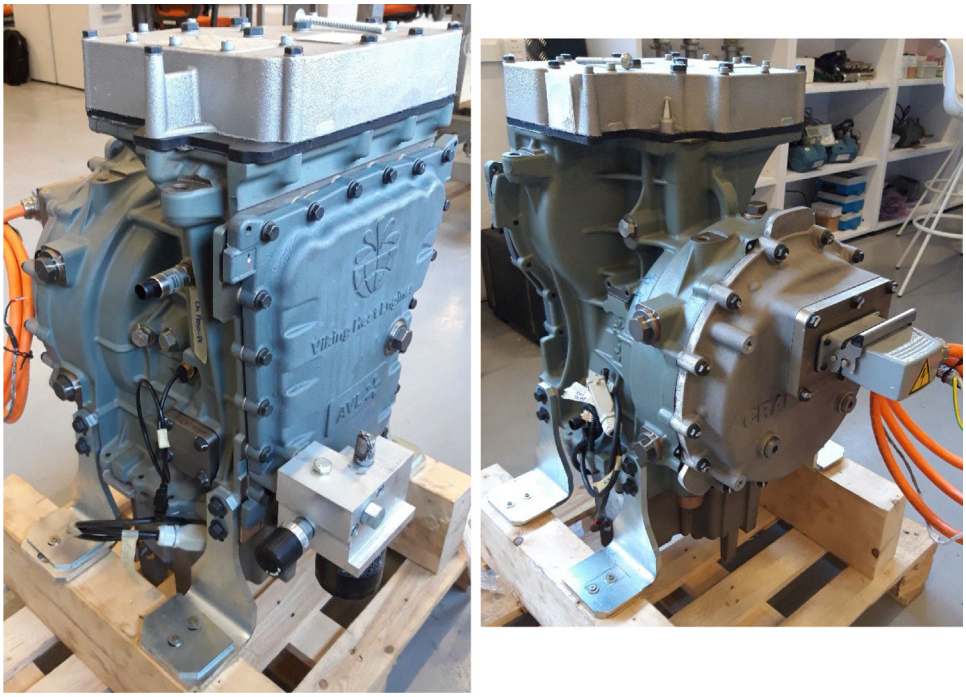

Fig. 4. Photographs of the VHE's HBC-511 compressor.

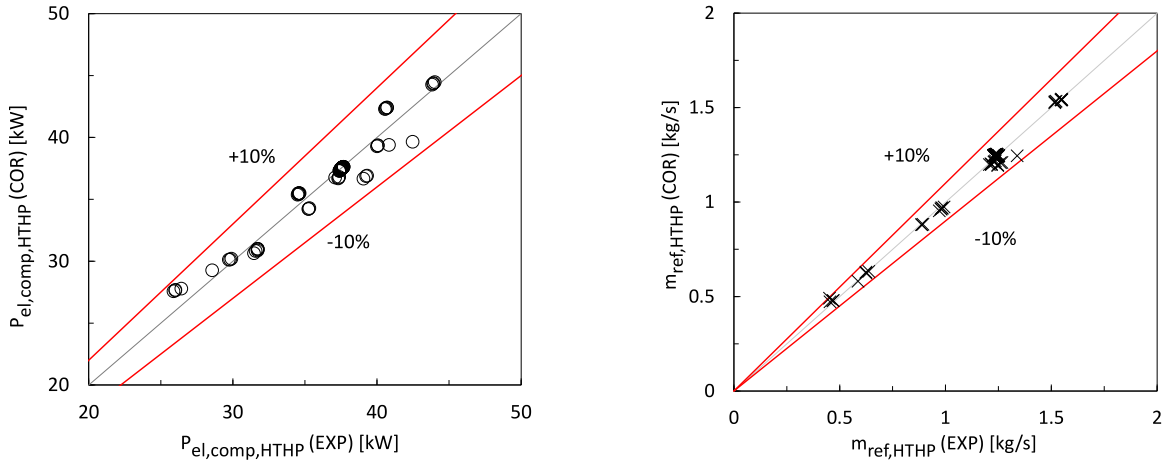

Fig. 5. Correlated (COR) vs. experimental (EXP) values of $P_{el,comp,HTHP}$(left) and $m_{ref,HTHP}$(right), for R-1336mzz(Z).

- The PP and the secondary fluid-side temperature lift inside the heat exchangers are fixed at 5 K.
- The isentropic efficiency values for the ORC's expander and pump are equal to 0.7.

To estimate the maximum capacity of the heat exchangers, the source and sink temperatures were fixed at 100 and 25 °C, respectively, and the maximum compressor speed, 1500 rpm, was maintained. Eqs. (1) and (2) were used to estimate the compressor's overall, volumetric, and isentropic efficiencies. The solution was obtained iteratively by varying the water mass flow rate inside the subcooler to guarantee that the sensible heat stored during the charging cycle is sufficient to preheat the refrigerant to the saturation temperature during the discharging process. This is an important design aspect to ensure that the refrigerant enters the tube bundle inside the LH-TES, as a saturated liquid to avoid, or at least mitigate, the maldistribution of refrigerant and the degradation of the heat transfer process inside the LH-TES.

Fig. 6 shows the simulation results of the EES-CHEST model for fixed $T_{src,in,HTHP}$, $T_{snk,in,ORC}$, $T_{melt,PCM}$, and $n_{comp,HTHP}$ of, respectively, 100 °C, 25 °C, 133 °C, and 1500 rpm. Under these working conditions, the input electrical power to the HTHP is 13.2 kW. Under these conditions, the HTHP's evaporator, condenser, and subcooler capacities are found to be 75.5, 44.8, and 41.4 kW, respectively. Thus, the capacities of the condenser and subcooler are similar. The subcooler, under these conditions, subcools the refrigerant by ≈73 K and heats the secondary fluid by ≈92 K.

SWEP International A.B. has provided the heat exchangers for the HTHP and ORC. SWEP's SSP G8 selecting tool was employed to size and select the required evaporator, condenser, and subcooler for the prototype. Table 3 summarizes the main specifications of the selected BPHXs.

3.4. Expansion device selection

To select an adequate expansion device, several requirements must be considered. The most important one is the operating

Table 3
Selected evaporator, condenser and subcooler for the HTHP.

Component	Evaporator	Condenser	Subcooler
Type		BPHX	
Manufacturer		SWEP	
Model	V200TH	B320HTL	B86H
No. of plates (NoP) [-]	70	100	50
Heat transfer Area [m^2]	8.77	12.2	2.88
Available overall heat transfer coefficient (OHTC) [W/m^2 K]	1450	824	1350
Hold-up volume [L] (ref./sec. fluid)	8.19/8.44	9.31/9.50	1.87/1.95
Height × Width × Depth [mm]	525 × 243 × 176.3	525 × 243 × 210	526 × 119 × 88
Weight [kg]	44.45	50.5	8.92

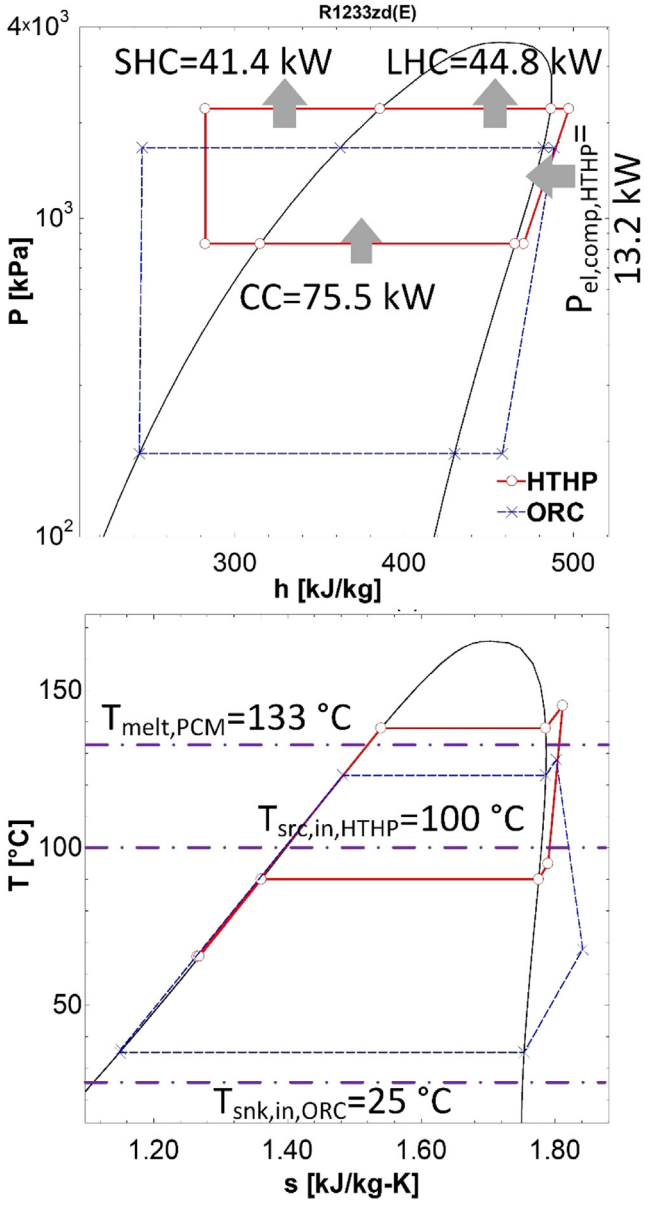

Fig. 6. EES-CHEST model results for $T_{src,in,HTHP} = 100$ °C and $T_{snk,in,ORC} = 25$ °C.

temperature range since the expansion device will operate at temperatures above 130 °C. Therefore, the selection criteria of the required expansion device were as follows:

- Capability to operate under high temperatures ≥ 130 °C.
- Suitability to work with R-1233zd(E).
- Programmable and electronically controlled.
- Fast opening and closing response.

According to the mentioned criteria, the selected valve is an electronic expansion device. The selected model is MVL661 (SIEMENS, 2021), which can operate up to 140 °C and is also suitable for R-1233zd(E). The valve can be controlled using electronic signals of 0–10 V and 4–20 mA, reaching an accuracy of 3% at full scale with a positioning time of 1 s Two selectable operating ranges are available for opening degrees of 0%–100% and 0%–63%.

3.5. Accessories selection

The selection of the liquid receiver depends on the estimated refrigerant charge according to the internal volume of the refrigerant loop, the operating temperatures, and the orientation within the prototype structure (Hundy et al., 2016). Considering the mentioned factors, the selected liquid receiver is a horizontal 40 liters capacity (RLHCY 400) made by Carly. The latter can withstand operating temperatures and pressures up to 140 °C and 68 bar, respectively (Carly, 2018a).

A suction accumulator has been mounted to protect the compressor from receiving liquid drops in the cylinder, particularly during partial load or after abrupt changes in the operating modes. The selected accumulator is an LCY 1011 model also from Carly, which can operate under high-temperature conditions (Carly, 2018b).

The HTHP has been designed knowing that it will be coupled in DLR with the LH-TES. This will increase both the volume and length of the refrigerant line. Therefore, an oil separator manufactured by Carly has been mounted at the discharge line of the compressor to retain the oil leaving the compressor and reduce oil migration.

Two refrigerant filters were mounted in the HTHP, one in the liquid line and the other in the compressor's suction. Both filters are of the BCY type from Carly (Carly, 2018c), which are fitted with special cartridges for filtering both liquid and vapor at high temperatures.

Additional auxiliary components such as valves, sight glasses, check valves, switches, ports, and sensors have been selected considering the working fluid, high-temperature conditions, and further operating characteristics of the HTHP.

3.6. Lubrication system

The lubricant used for this application has been selected and customized by the manufacturer considering the type of compressor, the working fluid, the operating temperatures, and pressures. The oil must withstand high temperatures while protecting the metallic parts which are in contact. In addition, the miscibility and solubility of the oil with the refrigerant have been considered to ensure oil return to the compressor, but also the content of refrigerant in the oil during stand-by stages (Hundy et al., 2016). FUCHS Schmierstoffe GmbH develops the lubricant with additives to overcome the mentioned harsh operating conditions resulting

Table 4
Heat transfer (HTC) and friction (FC) coefficients correlations used in IMST-ART simulations for BPHXs.

Component		Condenser	Evaporator
Refrigerant-side (single-phase) and secondary fluid-side	HTC	Dittus and Boelter (1930)[a]	
	FC	IMST-ART (2010)[b]	
Refrigerant-side (two-phase)	HTC	Shah (1979)[c]	Chen (1966)[d]
	FC	Friedel (1979)[e]	

[a]Adjusting the coefficients and the Reynolds number ranges in accordance with BPHXs.
[b]Proprietary correlation that correlates the FC against Reynolds number, taking into account some geometrical aspects of BPHXs.
[c]The original coefficients were re-fitted based on experimental data.
[d]Adjusting the HTC to some geometrical aspects of BPHXs.
[e]Based on single-phase friction factor for BPHXs.

in an oil with a kinematic viscosity of 310 mm tsup2/s at 40 °C (FUCHS, 2020).

The compressor is equipped with an external oil loop and a water-cooling loop, both designed and developed by TECNALIA. The oil collected at the oil separator passes through a filter and is redirected to the oil sump. The latter is located at the compressor's lower part, away from the compression chamber, to minimize overheating. In addition, both the electric motor and the lubricant of the compressor are cooled by a closed water loop. A water pump, a fan-coil radiator, and other auxiliary components are employed in this water loop.

4. HTHP model

The HTHP model was developed using the IMST-ART simulation tool. The latter has been developed by the Institute for Energy Engineering (IIE) at the Universitat Politècnica de València (UPV). IMST-ART is a commercial program that has been continuously developed for more than 20 years and has the capability to simulate individual heat pump components or stand-alone analysis, as well as the whole vapor compression cycle. Many articles in the literature show the IMST-ART's versatility and accurate validation against experimental tests (García-Cascales et al., 2007; Hassan et al., 2019; Pisano et al., 2015; Pitarch et al., 2019).

4.1. Heat exchangers modeling

IMST-ART includes an advanced heat exchanger sub-model based on the discretization of the heat exchanger in cells along the refrigerant and secondary fluid flow-direction, assuming one-dimensional flow. This sub-model can take into account both the heat transfer and pressure drop, with a local evaluation of the heat transfer coefficient and friction factor, using built-in correlations (Table 4) and the fluid thermo-physical properties. The model considers most of the geometrical and operation parameters of current evaporators and condensers. The inputs to the model are the HX's geometry, the refrigerant operating conditions (subcooling/superheat and mass flow rate), and the secondary fluid temperature lift.

The heat exchangers are discretized numerically, inside IMST-ART, based on the finite volume method (Patankar, 1980), along with the semi-explicit method for the wall temperature linked equation (SEWTLE), proposed by Corberán et al. (2001).

Table 5 shows that the IMST-ART's heat exchanger sub-model estimates accurately the performance of the selected evaporator and condenser. The absolute deviations in the condensation/evaporation temperatures are less than ±0.1 K, and less than ±0.5% regarding the thermal capacities. Fig. 7 shows the estimated temperature profiles inside the evaporator and condenser, and indicates the values and locations of the pinch points.

Table 5
IMST-ART estimated results vs. SWEP's catalog data for the selected evaporator and condenser.

Component	Parameter	SWEP	IMST-ART	Deviation
Evaporator (V200THx70)	$V_{ch,evap}$ [L]	7.383	7.382	±0.019%
	T_{evap} (dew) [°C]	92.940	92.901	±0.039 K
	$\Delta p_{ref,evap}$ [kPa]	5.660	5.724	±0.064 kPa
	Capacity [kW]	61.980	62.240	±0.419%
Condenser (B320HTLx100)	$V_{ch,cond}$ [L]	7.733	7.730	±0.038%
	T_{cond} (dew) [°C]	137.950	138.020	±0.070 K
	$\Delta p_{ref,cond}$ [kPa]	0.100	0.427	±0.327 kPa
	Capacity [kW]	46.370	46.349	±0.045%

4.2. Compressor modeling

For any compressor modeling, three main equations/correlations are required. The first correlation relates the mass flow rate, Eq. (1), to the compressor's volumetric efficiency ($\eta_{v,comp,HTHP}$) as follows:

$$\eta_{v,comp,HTHP} = \frac{m_{ref,HTHP}}{\rho_{suc} V_{disp}} \tag{3}$$

where ρ_{suc} is the refrigerant density at the suction [kg/m^3], and V_{disp} is the displacement volume [m^3/s]. $\eta_{v,comp,HTHP}$ indicates how efficiently the compressor can pump the theoretical volume flow rate.

The second correlation is the electrical power consumed, Eq. (2), which is used to calculate the compressor's overall efficiency ($\eta_{o,comp,HTHP}$) as indicated hereafter:

$$\eta_{o,comp,HTHP} = \frac{m_{ref,HTHP}\left(h_{dis,is} - h_{suc}\right)}{P_{el,comp,HTHP}} \tag{4}$$

where $h_{dis,is,}$ and h_{suc} are, respectively, the isentropic discharge and suction enthalpies [kJ/kg]. $\eta_{o,comp,HTHP}$ considers all the energy losses, electrical, mechanical, heat, etc., due to the conversion of electrical energy to internal thermal energy (compression of refrigerant).

Finally, an energy balance has been obtained in the compressor to account for the heat losses to the environment ($\varphi_{loss,comp,HTHP}$) relative to the electrical power consumption:

$$P_{el,comp,HTHP} = m_{ref,HTHP}\left(h_{dis} - h_{suc}\right) + Q_{loss,comp,HTHP} \tag{5}$$

$$Q_{loss,comp,HTHP} = \varphi_{loss,comp,HTHP} \cdot P_{el,comp,HTHP} \tag{6}$$

$$\varphi_{loss,comp,HTHP} = 1 - \frac{m_{ref,HTHP}\left(h_{dis} - h_{suc}\right)}{P_{el,comp,HTHP}} = 1 - \frac{\eta_{o,comp,HTHP}}{\eta_{is,comp,HTHP}} \tag{7}$$

$Q_{loss,comp,HTHP}$ are the heat losses to the environment [kW], and h_{dis} is the refrigerant enthalpy at the discharge [kJ/kg]. $\eta_{is,comp,HTHP}$ is the isentropic efficiency of the compressor [-], and shows how close the compression is to an isentropic, ideal, process. $\varphi_{loss,comp,HTHP}$ is an important factor that directly affects the discharge temperature.

Based on Eqs. (1) and (2), parametric tables of refrigerant mass flow rate and electrical power consumption are generated for different compressor speeds, suction and discharge pressures. In Eq. (1) M_{ref} was updated for R-1233zd(E), with $M_{R-1233zd(E)} = 130.5$ kg/kmol (Lemmon et al., 2018).

These tables are introduced in IMST-ART to estimate the three empirical parameters, $\eta_{v,comp,HTHP}$, $\eta_{o,comp,HTHP}$, and $\varphi_{loss,comp,HTHP}$, involved in Eq. (3), Eq. (4), and Eq. (7), respectively.

4.3. Connections and expansion devices modeling

IMST-ART takes into account the refrigerant flow in the discharge, liquid, and suction lines. The flow inside these lines is modeled as flow inside rounded pipes including a pressure drop

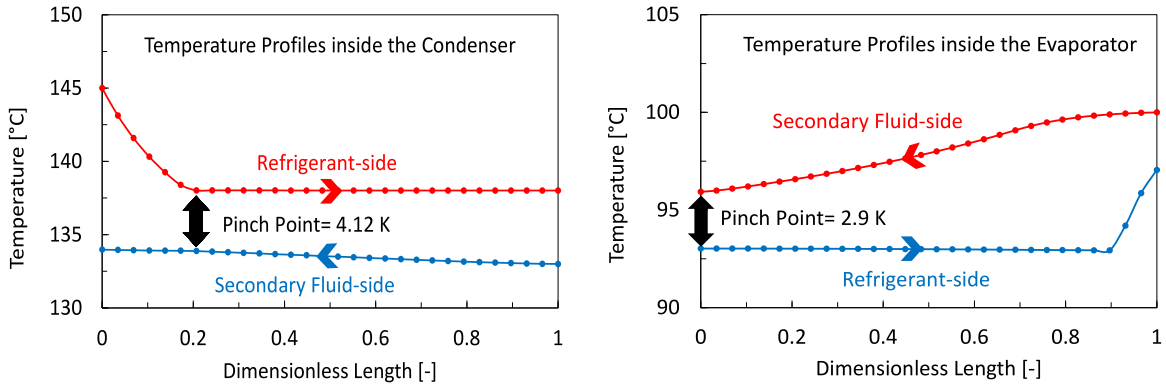

Fig. 7. Temperature profiles inside condenser (left) and evaporator (right).

and heat transfer to/from the surrounding. The heat transfer modeling is based on the classical ϵ-NTU method, considering the corresponding insulation, surrounding air temperature, and the mode of heat convection (natural or forced). The pressure drop is calculated, including friction, gravity, and acceleration effects. The pressure losses resulting from minor accessories, such as bends, junctions, check valves, etc., are also considered through the classical approach of equivalent length of pipe fittings.

Regarding the expansion devices, several options are available in IMST-ART: thermostatic or electronic expansion valve, capillary tube, and short tube. The model for thermostatic and electronic expansion valves used in the current HTHP is simple and assumes that the device can keep a constant superheat. Therefore, a specified superheat value at the evaporator outlet should be introduced as input in the heat pump cycle simulations. All expansion device models inside IMST-ART assume an isenthalpic expansion process, which in fact, is very close to reality.

4.4. Global heat pump model and solution method

The five main stages of the heat pump cycle solution/simulation inside IMST-ART are:

- *Stage 1: Inputs:*
  - Refrigerant and secondary fluids data: type, temperatures, flow rates.
  - Geometrical data for heat exchangers.
  - Compressor specifications and performance tables for mass flow rate and electrical power consumption as a function of n_{comp}, p_{suc}, and p_{dis}.
  - Heat pump working conditions: n_{comp}, SC, SH.
- *Stage 2: Discretization and Initialization of Variables:*
  - Compressor: generating tables for compressor's overall and volumetric efficiencies based on input performance tables.
  - Heat exchangers and tubes: discretizing into cells in the refrigerant flow direction and initializing the global variables for each cell.
- *Stage 3: Estimated Initial Solution for the Cycle:*
  - Estimating the evaporation and condensation temperatures/pressures, which are evaluated based on the input secondary fluids temperature lift values.
  - Using the compressor sub-model to estimate the mass flow rate of refrigerant based on the estimated pressure ratio and suction enthalpy.
  - Using the heat exchanger sub-model to calculate the outlet refrigerant enthalpy and pressure values from the evaporator and condenser.
- *Stage 4: Cycle Calculations:*
  - Each heat pump component has its dedicated sub-model to evaluate the outlet enthalpy, pressure, and/or mass flow rate at the current iteration (i) and compare against the values of the previous iteration ($i-1$) (Corberan and Gonzalvez).
  - A set of non-linear equations is achieved, in the form of: $f(x) = (x_{i-1} - x_i)/x_{estimated\ solution}$, where x is the desired outlet property.
  - This system of equations is solved using a standard solver based on the MINPACK subroutine HYBRD1 (Garbow, 1984), which adopts a modification of Powell's hybrid algorithm. This algorithm is a variation of Newton's method, which uses a finite-difference approximation to the Jacobian and takes precautions to avoid large step sizes or increasing residuals. For a detailed description of the method, refer to (Powell, 1977).
  - The Euclidean norm, square root of the sum of squares, of this set is adopted as the global convergence criteria (Corberan and Gonzalvez).
  - The heat exchanger's sub-model is based on the SEWTLE method, as mentioned in Section 4.1. The solution procedure starts with the initial estimation of the wall temperature field. Based on this, the refrigerant and secondary fluids properties are estimated by applying mass, energy, and momentum balances within each cell in the flow direction. The wall temperature field is updated based on the new estimation of fluids temperature fields. In the presence of longitudinal heat conduction (interaction between the current wall cell and neighboring four-wall cells), the wall governing equation involves five temperatures. The previous steps are repeated inside an internal iteration loop till finally reaching convergence. The convergence is achieved based on the residual of energy balance between the refrigerant- and secondary fluid-side.
- *Stage 5: Outputs:*
  - The cycle and components results are stored and shown to the user. This also allows exporting all the results to an external file.
  - The results include cycle representation on the p-h diagram, detailed temperature profiles and pressure

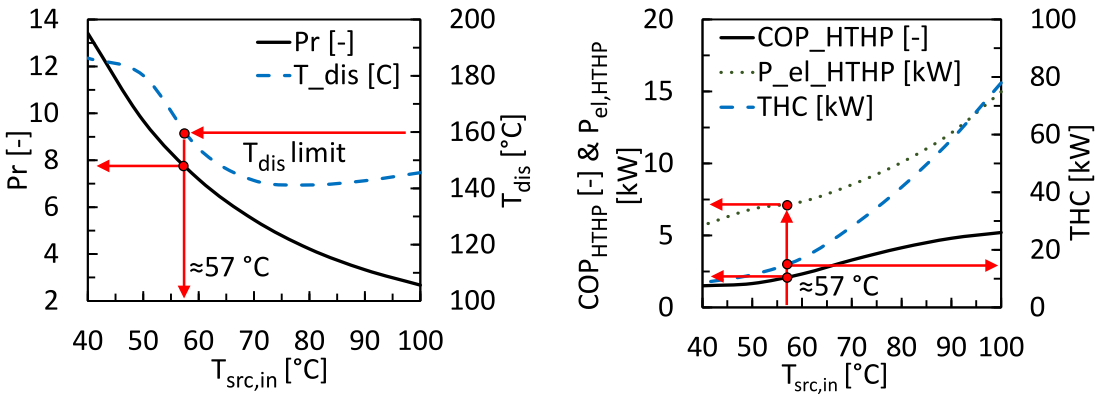

Fig. 8. The HTHP's main performance indicators vs. the source temperature range.

drop values inside heat exchangers, compressor performance, and overall performance parameters for the cycle under the given operating condition.

5. Parametric studies: Design and operating considerations

In this section, several parametric studies have been carried out with an emphasis on the following performance indicators:

- Heating coefficient of performance, including the consumption of auxiliaries (COP_{HTHP}).
- Sensible, latent, and total heating capacities (SHC, LHC, and THC).
- Total electrical power consumed by the HTHP, including the compressor and auxiliaries ($P_{el,HTHP}$).
- Discharge temperature (T_{dis}).
- Pressure ratio (Pr).
- Evaporation temperature (T_{evap}), and condensation temperature (T_{cond}).

In the current studies, the following parameters are fixed:

- The compressor's inverter efficiency is set to 90%, based on the manufacturer's catalog data (Viking Heat Engines, 2018).
- To account for the auxiliaries' consumption, the circulation pumps in the condenser, evaporator, and subcooler are assumed to have a typical efficiency of 30%.
- The condenser outlet is always saturated liquid to ensure a totally liquid refrigerant entering the subcooler.
- The temperature difference between the refrigerant inlet to the subcooler and the secondary fluid outlet is always fixed at 5 K.
- The temperature lift of the secondary fluid inside the evaporator is of 5 K.
- To reproduce the melting process of the PCM inside the LH-TES system, the inlet and outlet sink temperatures are kept constant at 133 and 134 °C, respectively, assuming a homogeneous melting process.

5.1. Possible heat source temperature range

As mentioned before, the main advantage of the CHEST system is the flexibility. The system can be integrated with any other energy storage system, district heating network, or even industrial facility. This yields a wide range of source temperatures between 40 and 100 °C. This study investigates the feasibility of operating the HTHP under this source temperature range. The compressor speed is fixed at 1500 rpm; the heat losses from the compressor are 28%, which is an average value from the manufacturer's data; the SH is constant at 10 K; and the inlet water temperature to the subcooler is at 60 °C.

As can be observed in Fig. 8(left), too low source temperatures lead to high pressure ratios (>10) and to unacceptable discharge temperatures (>160 °C). For source temperatures above 57 °C, the discharge temperatures remain below 160 °C and the pressure ratio is below 7.8.

Fig. 8 (right) shows that the HTHP can provide a total heating capacity (sensible and latent) from 78 kW, at $T_{src,in}$ = 100 °C, till 15 kW, at $T_{src,in}$ = 57 °C. For the same range of $T_{src,in}$, the total electrical power consumption starts at 15 kW and decreases down to ≈7 kW. This corresponds to a COP_{HTHP} that ranges from 5.2 down to 2.0.

Reaching a $T_{src,in}$ = 40 °C is infeasible since the Pr, T_{dis}, and COP_{HTHP} reach, respectively, values of 13.4, 186 °C, and 1.5. To reach this limit, a two-stage compression cycle or vapor injection technique would be required, which is out of the scope of the current work. Accordingly, the lower possible limit of $T_{src,in}$, for the chosen HTHP configuration, should be ≈60 °C, to ensure T_{dis} <160 °C and feasible Pr and COP_{HTHP} values.

5.2. Superheat optimization

The superheat of refrigerant before the inlet of the compressor is crucial. On the one hand, low values could result in the formation of liquid droplets at the inlet of the compressor, which can lead to wet compression and severe damage of the compressor. On the other hand, large values of SH, if they are achieved inside the evaporator, could result in a notable performance degradation due to the decrease of the evaporation temperature.

As mentioned before, using an IHX is impossible in the current HTHP configuration due to the need to store, as much as possible, the sensible heat from the refrigerant after the condensation. Thus, to achieve the required degree of SH, the only possible way is to superheat the refrigerant inside the evaporator. Subsequently, optimizing the SH value in the current study is important to ensure a good performance. To do so, two main aspects have been investigated. Firstly, the minimum required SH (SH_{min}) for the given range of $T_{src,in}$, based on a minimum desuperheating (DSH) limit at the inlet of condenser = 5 K, considering that the SH_{min} should be at least 3 K. Secondly, the maximum SH (SH_{max}) has also been obtained to ensure no more than ≈5% degradation in the COP_{HTHP} values compared to the values with SH_{min}.

Fig. 9a represents SH_{min} values as a function of the source temperatures. As the source temperature increases, SH_{min} increases up to a maximum value of 10.4 K at $T_{src,in}$ = 80 °C. For higher source temperatures in the range from 80–100 °C, lower SH_{min} values are obtained. This could be interpreted by the thermo-physical properties of the refrigerant and by the

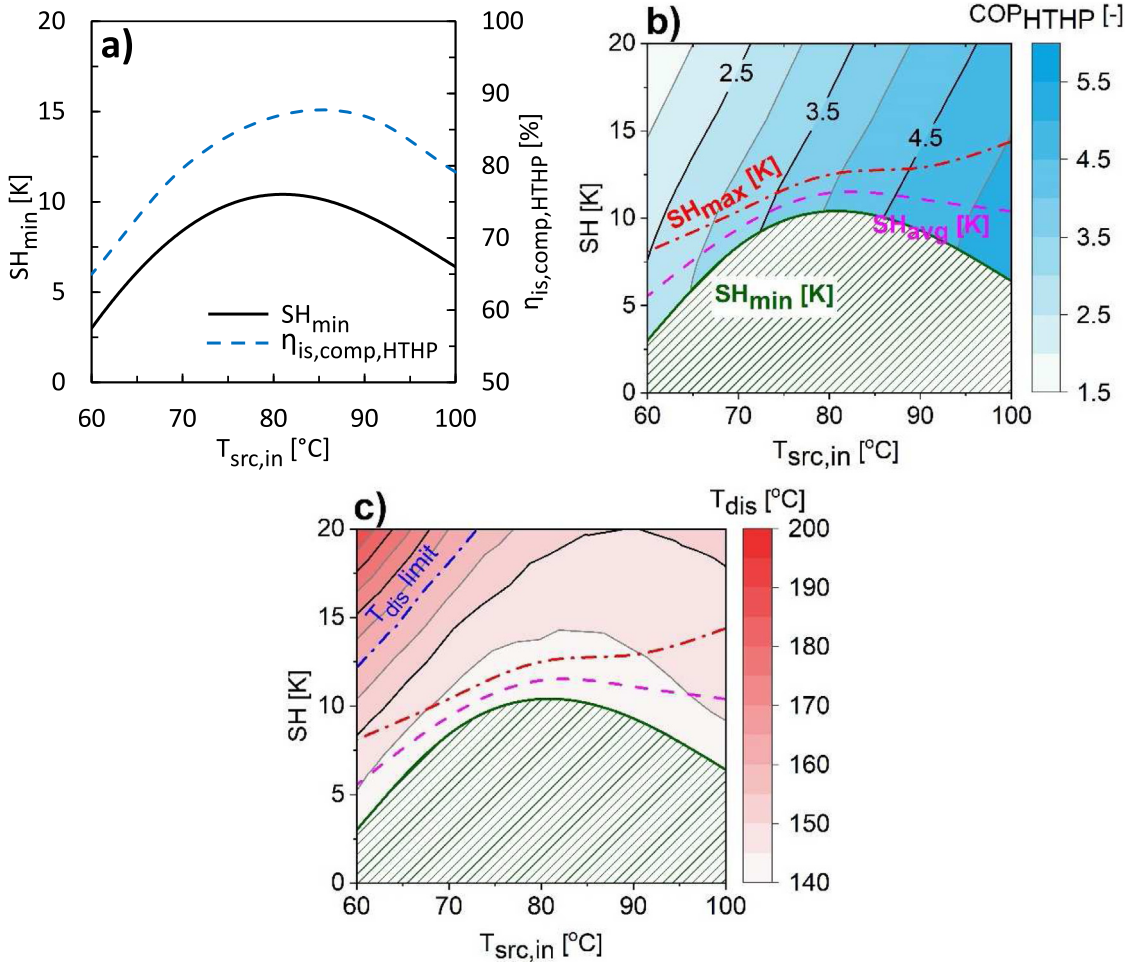

Fig. 9. (a) SH_{min} required and corresponding $\eta_{is,comp,HTHP}$ for the given range of $T_{src,in}$, (b) contours of COP_{HTHP}, and (c) T_{dis} values as a function of $T_{src,in}$ and SH.

behavior of $\eta_{is,comp,HTHP}$, which reaches a maximum of 87% for a source temperature of around 85 °C. The lower the $\eta_{is,comp,HTHP}$, the higher the discharge temperature, and the lower the SH_{min} required to prevent the wet compression. One of the primary important factors affecting the $\eta_{is,comp,HTHP}$ is the heat losses from the compressor (Eq. (7)); this effect will be discussed later.

Fig. 9b and Fig. 9c show the maps of the COP_{HTHP} and T_{dis} as a function of $T_{src,in}$, and SH. As can be seen, the T_{dis} values range between 141 and 143 °C. At $T_{src,in} = 60$ °C, the COP_{HTHP} is of 2.62, and it increases until a value of 5.30 at $T_{src,in} = 100$ °C. The maximum margin to increase the SH, which results in a 5% reduction in COP_{HTHP}, can also be seen in Fig. 9b and c. The difference between the SH_{max} and SH_{min} is minimum (≈1.6 K) for $T_{src,in}$≈ 77–72 °C and can reach up to 5.1 K, at $T_{src,in} = 60$ °C, or even 8 K, at $T_{src,in} = 100$ °C. In the following studies, the SH value assigned for each $T_{src,in}$, will be the average (SH_{avg}), as indicated in Fig. 9b.

5.3. Compressor's heat losses

The heat losses from the compressor to the environment impact directly the discharge temperature and, subsequently, the isentropic efficiency of the compressor, as indicated in Eq. (7). Based on the experimental data provided by the compressor's manufacturer, the average heat losses $\varphi_{loss,comp,HTHP}$ was 28%, with a minimum value of 22% and a maximum value of 43%. However, this depends on whether the compressor is insulated or not, on the pressure ratio, the ambient temperature, and the flow rate of cooling water/air (if this option is available). The current study investigates the effect of increasing the $\varphi_{loss,comp,HTHP}$, from 15% to 45%, on the compressor and cycle performance.

Fig. 10a shows that, at any given $T_{src,in}$, increasing the $\varphi_{loss,comp,HTHP}$ decreases the discharge temperature significantly until reaching approximately the saturation temperature at the corresponding discharge pressure. This results in $\eta_{is,comp,HTHP}$ values higher than 100%, especially for $\varphi_{loss,comp,HTHP} > 40\%$ and $T_{src,in} > 74$ °C, as seen in Fig. 10b. For $\varphi_{loss,comp,HTHP} \geq 45\%$, the results indicate that for all $T_{src,in}$ values the DSH is less than 5 K, and approaches zero at low values of $T_{src,in}$. This is not a favorable scenario since very low discharge temperatures could result in wet compression. To avoid this, the SH should be increased, and this could lead to a significant degradation in the HTHP's performance, as discussed previously, especially if the SH increased beyond the SH_{max} limit. As an example, for $T_{src,in} = 80$ °C and $SH_{avg} = 11.5$ K, increasing the $\varphi_{loss,comp,HTHP}$ from 15% to 45% decreases the DSH value, at the inlet of condenser, from 10.3 to 0.82 K, respectively. This could lead to condensation of the refrigerant at the outlet of the compressor. To avoid this and to maintain a minimum DSH of 5 K, the SH, in this case, should be increased to be 16.8 K. This results in a decrease of T_{evap} by 5.3 K, and degradation of the COP_{HTHP} by ≈12.3%.

At constant SH value, usually, the increase of the $\varphi_{loss,comp,HTHP}$ hardly affects the $\eta_{o,comp,HTHP}$, or COP_{HTHP}. Based on the current results, the recommendation is to maintain the $\varphi_{loss,comp,HTHP} \leq 35\%$ to avoid wet compression or to increase the SH value. This could be guaranteed with proper compressor insulation and adequate control of the compressor's cooling water/air circulation rate.

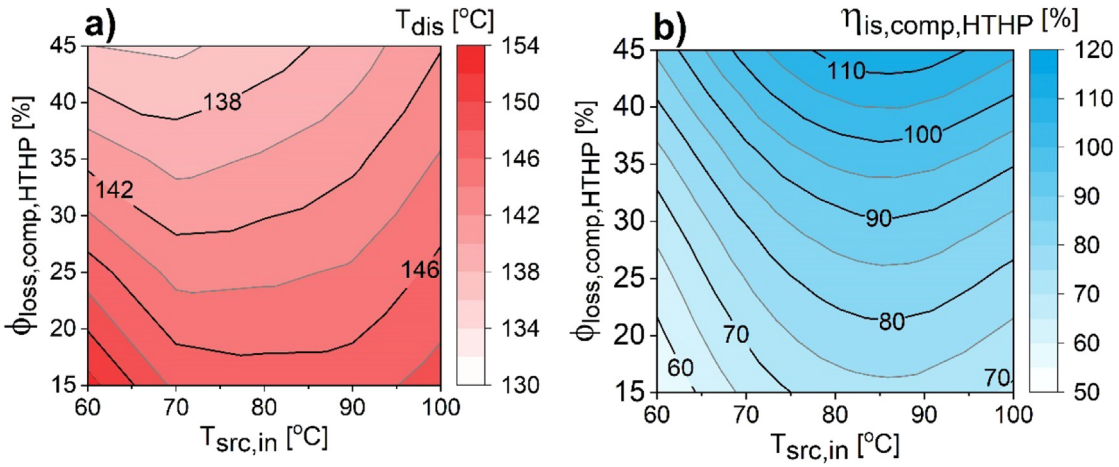

Fig. 10. Contours of (a) T_{dis}, and (b) $\eta_{is,comp,HTHP}$, as function of $T_{src,in}$ and $\varphi_{loss,comp,HTHP}$.

5.4. Inlet water temperature range to the subcooler

As mentioned before, the subcooler of the HTHP is an essential component that is used to transfer the sensible heat from the refrigerant to the water loop by subcooling the saturated liquid refrigerant out from the condenser. Based on the preliminary requirements for the CHEST system, the inlet water temperature to the subcooler should be ranged between 40 and 80 °C (Pascual, 2019). This is the expected range for the pressurized water stored in the sensible heat storage after the previous discharging cycle. In all the previous studies, this temperature was fixed at 60 °C, as an average value within this range; however, in the current study, the effect of changing this temperature is further investigated.

As seen in Fig. 11a, Fig. 11b, and Fig. 11c, generally, at any given $T_{src,in}$, increasing the $T_{w,in,subc}$ results in a decrease in the total subcooling inside the subcooler (SC_{subc}); subsequently, the total heating capacity THC, which in turn, results in a reduction in the COP_{HTHP}. For example, at the nominal point, where $T_{src,in} = 80$ °C, increasing the $T_{w,in,subc}$ from 60 to 80 °C results in a decrease in the SC_{subc} by 16 K and THC by 10.1%. The COP_{HTHP} decreases from 4.0 to 3.6. In contrast, reducing $T_{w,in,subc}$ from 60 to 40 °C results in an increase in the SC_{subc} and THC, respectively, by 15.7 K and 9.6%, and the COP_{HTHP} increases to be 4.4.

Thus, the lower the inlet water temperature to the subcooler, the higher the HTHP's performance. However, the main limit for working under low $T_{w,in,subc}$ values is the $m_{w,subc}$. Fig. 11d shows that, in the current study, for $T_{src,in}$ values less than 70 °C, and for a given $T_{w,in,subc}$ less than 60 °C, the required mass flow rate of water could reach very low values, <150 kg/h. This could present a challenge for system stability and control. Finally, as a recommendation, it is better for the system maintaining the $T_{w,in,subc}$ as low as possible, keeping in mind a minimum $m_{w,subc}$ value of 150 kg/h.

5.5. HTHP's partial load

The proposed HTHP, once integrated into the full CHEST system, would not always run at full load. The partial load scenarios could also occur depending on the state of the charge (SoC) of the HT-TES system, or on the availability of electrical power from the RES to drive the compressor. To match the HTHP load with the SoC of the HT-TES system at given source and sink temperatures, the only parameter that can be controlled is the compressor speed $n_{comp,HTHP}$. Changing the $n_{comp,HTHP}$, implies changing the mass flow rate of refrigerant; and, subsequently, the total heating capacity of the HTHP. Based on the compressor's manufacturer, the current compressor has a speed range from 500 to 1500 rpm (Table 2). The effect of varying $n_{comp,HTHP}$ on the HTHP's global performance is evaluated, in detail, in the current section. In this study, average values were fixed for the inlet water temperature to the subcooler and compressor's heat losses percentage.

Fig. 12 presents a performance map for the current HTHP as function of $T_{src,in}$ and $n_{comp,HTHP}$, at constant $T_{w,in,subc} = 60$ °C. For the given range of the $n_{comp,HTHP}$, Fig. 12a shows that the HTHP consumes electrical power from 2.6 kW, at $n_{comp,HTHP} = 500$ rpm and $T_{src,in} = 60$ °C, to 15 kW, at $n_{comp,HTHP} = 1500$ rpm and $T_{src,in} = 100$ °C. This corresponds to a LHC that ranges from 3.9 to 43 kW (Fig. 12b); and SHC that varies from 3.3 to 34.4 kW (Fig. 12c). Fig. 12d indicates that at any given $T_{src,in}$ increasing the $n_{comp,HTHP}$ reduces the COP_{HTHP}. For example, by increasing the $n_{comp,HTHP}$ from 500 to 1500 rpm, the COP_{HTHP} reduces by 13%, 6.1%, and 7.5% for $T_{src,in} = 100$, 80, and 60 °C, respectively. The maximum COP_{HTHP} achieved is 5.9, at $n_{comp,HTHP} = 500$ rpm and $T_{src,in} = 100$ °C; while the minimum value is 2.6, at $n_{comp,HTHP} = 1500$ rpm and $T_{src,in} = 60$ °C. As discussed before in Section 5.4, reducing as minimum as possible the $T_{w,in,subc}$ has a positive impact on the system's performance. Accordingly, reducing the $T_{w,in,subc}$ from 60 to 40 °C increases the maximum COP_{HTHP} value by 9.7% and the minimum COP_{HTHP} value by 7.7%.

As also seen in Fig. 12d, to maintain a typical value of $COP_{HTHP} \geq 4.0$ at any given $n_{comp,HTHP}$ the $T_{src,in}$ should always be ≥80 °C.

The current compressor could face some difficulties running stable at speeds below 800–900 rpm due to vibration and control issues. However, the minimum $n_{comp,HTHP}$ value will be specified more accurately during the experimental campaign.

6. Conclusions and suggestions

The current paper presents the detailed design and potential performance of a HTHP developed within the European project CHESTER. The design of the condenser and subcooler is not straightforward since the HTHP has been conceived to store both latent and sensible heat. Once integrated in the full CHEST system at DLR, the heat pump will be the first-of-its-kind experimental demonstrator of a compressed heat energy storage system. The main conclusions and suggestions of the present work are:

- R-1233zd(E) was selected for the current HTHP prototype. Compared with the reference refrigerant R-245fa, R-1233zd(E) shows higher T_{crit}, by 13 K, similar COP, VHC, and Pr values, besides, being a non-flammable and non-toxic refrigerant with very low GWP value of ≈1.

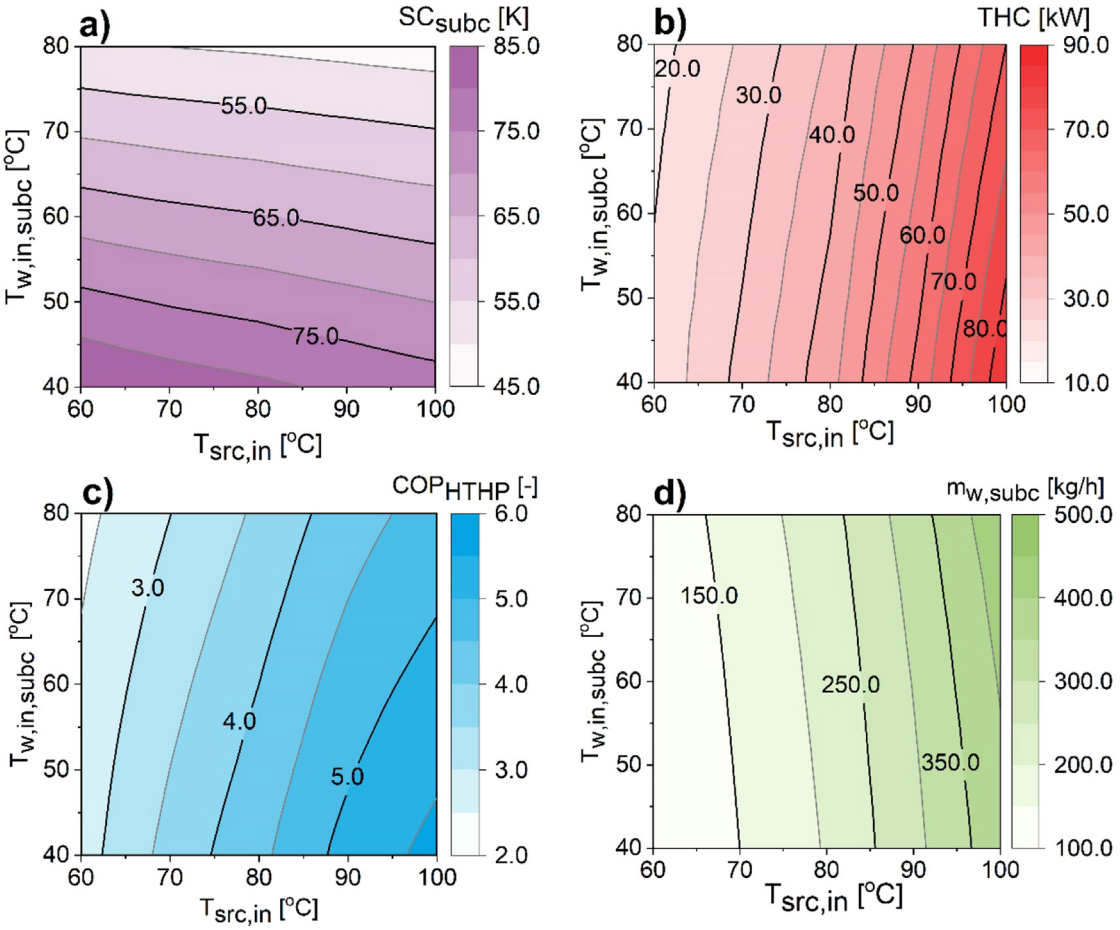

Fig. 11. Effect of varying $T_{w,in,subc}$ in (a) SC_{subc}, (b) THC, (c) COP_{HTHP}, and (d) $m_{w,subc}$.

- The simulation results suggest that the minimum $T_{src,in}$ for the proposed HTHP should not be lower than 60 °C. This is necessary to obtain a reasonable performance in terms of COP_{HTHP} and Pr, and $T_{dis} < 160$ °C, which is the limit of the current compressor.
- For each given $T_{src,in}$ there is a minimum SH value (SH_{min}) which yields the highest COP_{HTHP}, while ensuring dry compression. The SH_{min} reaches its maximum value of 10.4 K at $T_{src,in} = 80$ °C, and its lowest value of 3 K at $T_{src,in} = 60$ °C. This behavior is due to the trend of $\eta_{is,comp,HTHP}$ with respect to $T_{src,in}$. Based on this, the authors suggest maintaining the SH value as low as possible to avoid system degradation.
- The main factor that affects the $\eta_{is,comp,HTHP}$ is the percentage of heat losses from the compressor to the environment ($\varphi_{loss,comp,HTHP}$). The simulation results indicate that the thermal losses should be kept $\leq$35% to avoid wet compression and increasing the SH value that could degrade the system's performance.
- One of the main parameters that affect the current HTHP's performance is the inlet water temperature to the subcooler. The results show that the lower the $T_{w,in,subc}$, the higher the COP_{HTHP}. However, the authors recommend keeping a minimum water mass flow rate inside the subcooler of 150 kg/h to ensure stable behavior. The recommended range of $T_{w,in,sub}$ is 40–60 °C.
- Finally, the partial load scenarios were considered by changing the compressor's speed. The results show that the $T_{src,in}$ should always be $\geq$80 °C to maintain a $COP_{HTHP} \geq 4.0$ at any given $n_{comp,HTHP}$ value. By increasing the $n_{comp,HTHP}$ from 500 to 1500 rpm, the current HTHP, at the nominal point where $T_{src,in} = 80$ °C and $T_{w,in,subc} = 60$ °C, consumes an electrical power from 3.23 up to 9.88 kW, delivers LHC from 7.40 up to 21.59 kW and SHC from 6.35 up to 17.94 kW. This corresponds to a COP_{HTHP} between 4.0 at 1500 rpm and 4.3 at 500 rpm.

The current results, conclusions, and suggestions represent a roadmap for designing, sizing, and mapping the performance of HTHPs integrated in pumped thermal energy storage (PTES) systems. The continuation of this work will include the experimental results of the presented HTHP configuration, the full model validation, and global performance maps/corrections.

Declaration of competing interest

The authors declare that they have no known competing financial interests or personal relationships that could have appeared to influence the work reported in this paper.

Data availability

The authors do not have permission to share data.

Acknowledgments

- This work has been partially funded by grant agreement No. 764042 (CHESTER project) of the European Union's Horizon 2020 research and innovation program.
- The authors would like to express their deep gratitude to Prof. Dr. Jose Miguel Corberán Salvador for his perseverance, encouragement, and invaluable guidance during this work.

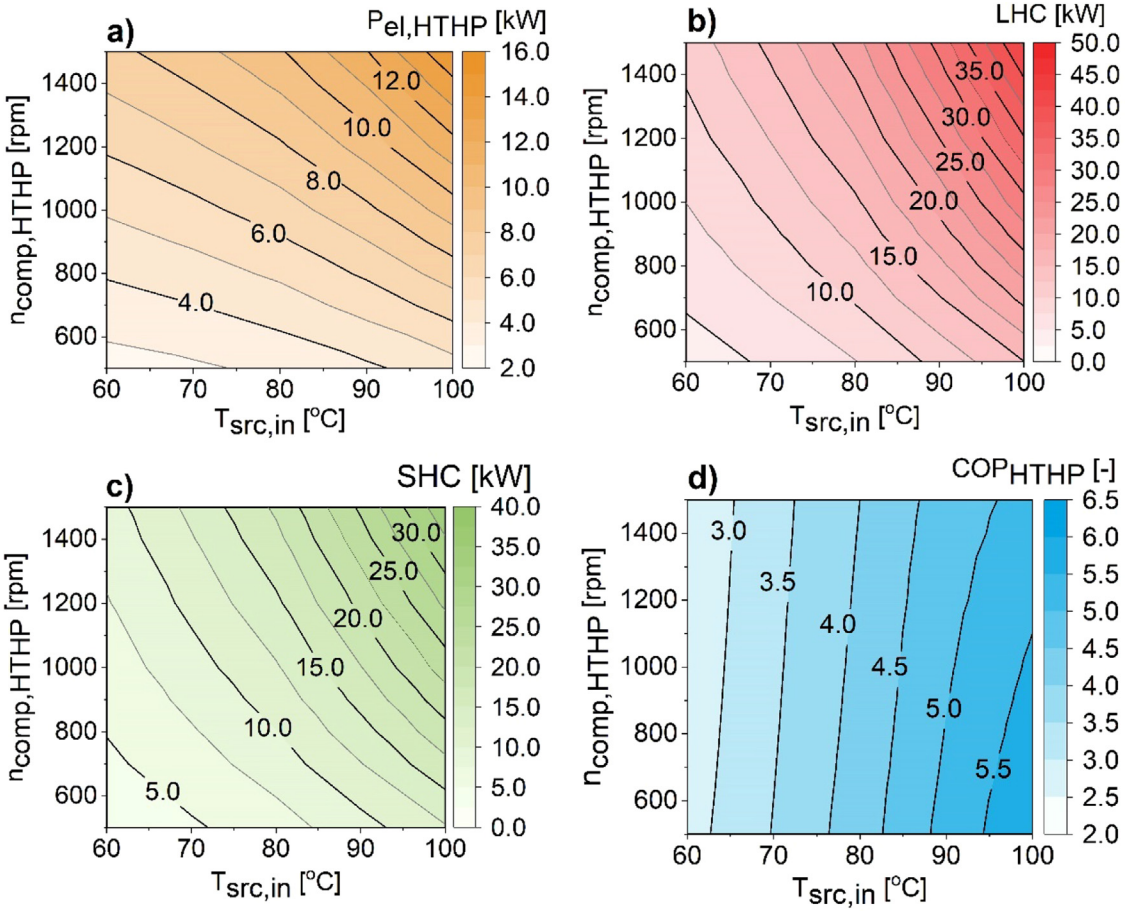

Fig. 12. HTHP's performance under partial loads and constant $T_{w,in,subc} = 60$ °C, where (a) $P_{el,HTHP}$, (b) LHC, (c) SHC, and (d) COP_{HTHP}.

References

al Shaqsi, A.Z., Sopian, K., Al-Hinai, A., 2020. Review of energy storage services, applications, limitations, and benefits. Energy Rep. http://dx.doi.org/10.1016/j.egyr.2020.07.028.

Arpagaus, C., Kuster, R., Prinzing, M., Bless, F., Uhlmann, M., Buchel, E., Frei, S., Schiffmann, J., Bertsch, Stefan S., 2019. High temperature heat pump using HFO and HCFO refrigerants – system design and experimental results. In: ICR 2019, the 25th IIR International Congress of Refrigeration, August 24-30. Montréal, Québec, Canada.

ASHRAE, 2016. Standard 34-safety standard for refrigeration systems and designation and classification of refrigerants.

Bamigbetan, O., Eikevik, T.M., Nekså, P., Bantle, M., Schlemminger, C., 2019. Experimental investigation of a prototype R-600 compressor for high temperature heat pump. Energy 169, 730–738. http://dx.doi.org/10.1016/j.energy.2018.12.020.

Barnoon, P., 2021. Modeling of a high temperature heat exchanger to supply hydrogen required by fuel cells through reforming process. Energy Rep. 7, 5685–5699. http://dx.doi.org/10.1016/j.egyr.2021.08.171.

Barnoon, P., Toghraie, D., Mehmandoust, B., Fazilati, M.A., Eftekhari, S.A., 2022. Natural-forced cooling and Monte-Carlo multi-objective optimization of mechanical and thermal characteristics of a bipolar plate for use in a proton exchange membrane fuel cell. Energy Rep. 8, 2747–2761. http://dx.doi.org/10.1016/j.egyr.2022.01.199.

Carly, 2018a. Liquid receivers RLHCY and RLVCY (product manual).

Carly, 2018b. Suction line accumulators LCY, LCYE, and LCY-ST (product manual).

Carly, 2018c. Replaceable core filter drier shells BDCY, BCYm and BCY-HP (product manual).

Chen, J.C., 1966. Correlation for boiling heat transfer to saturated fluids in convective flow. Ind. Eng. Chem. Process Des. Dev. 5, 322–329. http://dx.doi.org/10.1021/i260019a023.

Corberán, J.M., de Córdoba, P.F., Gonzálvez, J., Alias, F., 2001. Semiexplicit method for wall temperature linked equations (SEWTLE): A general finite-volume technique for the calculation of complex heat exchangers. Numer. Heat Transfer B 40, 37–59. http://dx.doi.org/10.1080/104077901300233596.

Corberan, J.M., Gonzalvez, J., 1998. The matching problem on the modeling of vapor compression Systems. In: International Refrigeration and Air Conditioning Conference at Purdue.

Corberán, J.M., Hassan, A.H., Payá, J., 2019. Thermodynamic analysis and selection of refrigerants for high-temperature heat pumps. In: Refrigeration Science and Technology. International Institute of Refrigeration, pp. 4705–4712. http://dx.doi.org/10.18462/iir.icr.2019.1193.

Dascalu, A., Sharkh, S., Cruden, A., Stevenson, P., 2022. Performance of a hybrid battery energy storage system. Energy Rep. 8, 1–7. http://dx.doi.org/10.1016/j.egyr.2022.05.040.

de-Boer, R., Marina, A., Zühlsdorf, B., Arpagaus, C., Bantle, M., Wilk, V., Elmegaard, B., Corberán, J., Benson, J., 2020. Strengthening industrial heat pump innovation: Decarbonizing industrial heat.

Dittus, F.W., Boelter, L.M.K., 1930. Heat Transfer in Automobile Radiators of the Tubular Type. Vol. 2, University of California Publications in Engineering, pp. 443–461.

Doretti, L., Martelletto, F., Mancin, S., 2020. Numerical analyses of concrete thermal energy storage systems: effect of the modules' arrangement. Energy Rep. 6, 199–214. http://dx.doi.org/10.1016/j.egyr.2020.07.002.

EDF, 2015. Heat pumps for industrial waste recovery (R&D report).

Feng, L., Zhang, X., Li, X., Li, B., Li, Y., Xu, Y., Guo, H., Zhou, X., Chen, H., 2022. Performance analysis of hybrid energy storage integrated with distributed renewable energy. Energy Rep. 8, 1829–1838. http://dx.doi.org/10.1016/j.egyr.2021.12.078.

Fleckel, T., 2015. Performance testing of a lab-scale high temperature heat pump with HFO-1336mzz-z as the working fluid. In: European Heat Pump Summit. Nuremberg.

Fleckl, T., Hartl, M., Helminger, F., Kontomaris, K., 2015. Performance testing of a lab-scale high temperature heat pump with HFO-1336mzz-z as the working fluid. In: European Heat Pump Summit 2015, October 20-21. Nuremberg, Germany.

Friedel, L., 1979. New friction pressure drop correlations for upward, horizontal, and downward two-phase pipe flow. In: HTFS Symposium. Oxford.

FUCHS, 2020. RENISO: Refrigeration oils 2020/2021 (product brochure).

Garbow, B.S., 1984. MINPACK-1, Subroutine Library for Nonlinear Equation System, Mathematics and Computer Science Division. Argonne National Laboratory, Argonne, Illinois.

García-Cascales, J.R., Vera-García, F., Corberán-Salvador, J.M., Gonzálvez-Maciá, J., 2007. Assessment of boiling and condensation heat transfer correlations in the modelling of plate heat exchangers. Int. J. Refrig. 30, 1029–1041. http://dx.doi.org/10.1016/j.ijrefrig.2007.01.004.

Gluyas, J.G., Adams, C.A., Wilson, I.A.G., 2020. The theoretical potential for large-scale underground thermal energy storage (UTES) within the UK. Energy Rep. 6, 229–237. http://dx.doi.org/10.1016/j.egyr.2020.12.006.

Hassan, A.H., Martínez-Ballester, S., Gonzálvez-Maciá, J., 2019. Comparison of different modeling approaches for minichannel evaporators under dehumidification. Heat Mass Transfer 55, 2901–2919. http://dx.doi.org/10.1007/s00231-019-02622-0.

Hassan, A.H., O'Donoghue, L., Sánchez-Canales, V., Corberán, J.M., Payá, J., Jockenhöfer, H., 2020. Thermodynamic analysis of high-temperature pumped thermal energy storage systems: Refrigerant selection, performance and limitations. Energy Rep. 6, 147–159. http://dx.doi.org/10.1016/j.egyr.2020.05.010.

Huang, R., Li, Z., Hong, W., Wu, Q., Yu, X., 2020. Experimental and numerical study of PCM thermophysical parameters on lithium-ion battery thermal management. Energy Rep. 6, 8–19. http://dx.doi.org/10.1016/j.egyr.2019.09.060.

Hundy, G.F., Trott, A.R., Welch, T.C., 2016. Refrigeration, Air Conditioning and Heat Pumps, fifth ed. Butterworth-Heinemann, http://dx.doi.org/10.1016/B978-0-08-100647-4.00008-5.

IMST-ART, 2010. Simulation Tool to Assist the Selection, Design and Optimization of Refrigeration Equipment and Components [WWW Document]. Instituto Universitario de Investigación en Ingeniería Energética, Universitat Politècnica de València, Valencia, URL http://www.imst-art.com/.

Kaida, T., Sakuraba, I., Hashimoto, K., Hasegawa, H., 2015. Experimental performance evaluation of heat pump-based steam supply system. In: IOP Conference Series: Materials Science and Engineering. Institute of Physics Publishing, http://dx.doi.org/10.1088/1757-899X/90/1/012076.

Klein, S.A., 2019. Engineering Equation Solver (Version V10.643).

Kosmadakis, G., 2019. Estimating the potential of industrial (high-temperature) heat pumps for exploiting waste heat in EU industries. Appl. Therm. Eng. 156, 287–298. http://dx.doi.org/10.1016/j.applthermaleng.2019.04.082.

Kosmadakis, G., Arpagaus, C., Neofytou, P., Bertsch, S., 2020. Techno-economic analysis of high-temperature heat pumps with low-global warming potential refrigerants for upgrading waste heat up to 150 °C. Energy Convers. Manage. 226. http://dx.doi.org/10.1016/j.enconman.2020.113488.

Lemmon, E.W., Bell, I.H., Huber, M.L., McLinden, M.O., 2018. NIST Standard Reference Database 23: Reference Fluid Thermodynamic and Transport Properties-REFPROP, Version 10.0. National Institute of Standards and Technology, Standard Reference Data Program, Gaithersburg.

Li, S., He, S., Song, W., Feng, Z., 2021. Thermodynamic analysis of the heat pump steam system with medium-low temperature heat source. Energy Rep. 7, 266–278. http://dx.doi.org/10.1016/j.egyr.2021.10.032.

Lu, Y., Chen, H., Wang, L., Yu, Z., Huang, Y., Yu, X., Wang, Y., Roskilly, A.P., 2021. Energy storage driving towards a clean energy future. Energy Rep. http://dx.doi.org/10.1016/j.egyr.2021.02.040.

Mateu-Royo, C., Navarro-Esbrí, J., Mota-Babiloni, A., Molés, F., Amat-Albuixech, M., 2019. Experimental exergy and energy analysis of a novel high-temperature heat pump with scroll compressor for waste heat recovery. Appl. Energy 253, 113504. http://dx.doi.org/10.1016/j.apenergy.2019.113504.

MAYEKAWA, 2022. Eco sirocco (CO2 heat pump air heater) [WWW Document]. URL https://www.mayekawa.com.au/products/heat-pumps/eco-sirocco/ (accessed 1.21.22).

Mei, B., Barnoon, P., Toghraie, D., Su, C.H., Nguyen, H.C., Khan, A., 2022. Energy, exergy, environmental and economic analyzes (4E) and multi-objective optimization of a PEM fuel cell equipped with coolant channels. Renew. Sustain. Energy Rev. 157. http://dx.doi.org/10.1016/j.rser.2021.112021.

Meng, Y., Zhou, R., Dinçer, H., Yüksel, S., Wang, C., 2021. Analysis of inventive problem-solving capacities for renewable energy storage investments. Energy Rep. 7, 4779–4791. http://dx.doi.org/10.1016/j.egyr.2021.06.086.

Nilsson, M., Nes Rislå, H., Kontomaris, K., 2017. Measured performance of a novel high temperature heat pump with HFO-1336mzz(z) as the working fluid. In: 12th IEA Heat Pump Conference 2017. Rotterdam.

OCHSNER, 2022. OCHSNER energy technology: Heat pumps for high outputs [WWW Document]. URL https://www.ochsner.com/en/ochsner-products/high-capacity-heat-pumps/ (accessed 1.21.22).

Papapetrou, M., Kosmadakis, G., Cipollina, A., la Commare, U., Micale, G., 2018. Industrial waste heat: Estimation of the technically available resource in the EU per industrial sector, temperature level and country. Appl. Therm. Eng. 138, 207–216. http://dx.doi.org/10.1016/j.applthermaleng.2018.04.043.

Pascual, C., 2019. D2.4. Requirements of individual technologies that form the CHEST system, CHESTER EU Project (No. 764042), https://www.chester-project.eu/.

Patankar, S.V., 1980. Numerical Heat Transfer and Fluid Flow, Electro Skills Series. Hemisphere Publishing Corporation.

Pisano, A., Martínez-Ballester, S., Corberán, J.M., Mauro, A.W., 2015. Optimal design of a light commercial freezer through the analysis of the combined effects of capillary tube diameter and refrigerant charge on the performance. Int. J. Refrig. 52, 1–10. http://dx.doi.org/10.1016/j.ijrefrig.2014.12.023.

Pitarch, M., Hervas-Blasco, E., Navarro-Peris, E., Corberán, J.M., 2019. Exergy analysis on a heat pump working between a heat sink and a heat source of finite heat capacity rate. Int. J. Refrig. 99, 337–350. http://dx.doi.org/10.1016/j.ijrefrig.2018.11.044.

Powell, M.J.D., 1977. Restart procedures for the conjugate gradient method. Math. Program. 12, 241–254. http://dx.doi.org/10.1007/BF01593790.

Shah, M.M., 1979. A general correlation for heat transfer during film condensation inside pipes. Int. J. Heat Mass Transfer 22, 547–556. http://dx.doi.org/10.1016/0017-9310(79)90058-9.

SIEMENS, 2021. Modulating refrigerant valves with magnetic actuator, PS45-MVL661 (product manual).

SPH, 2022. SPH sustainable process heat [WWW Document]. URL https://www.spheat.de/?lang=en (accessed 1.21.22).

SWEP International AB, 2019. SWEP SSP G8 (V. 2019.619.2.0).

Viking Heat Engines, 2018. HBC-511: Piston compressor for industrial heat pumps (data sheet).